ACS Catalysis

Research Article

pubs.acs.org/acscatalysis

Analysis of the Promoted Activity and Molecular Mechanism of Hydrogen Production over Fine Au−Pt Alloyed TiO_2 Photocatalysts

Fenglong Wang,[†] Yijiao Jiang,*[,‡] Douglas J. Lawes,[§] Graham E. Ball,[∥] Cuifeng Zhou,[⊥] Zongwen Liu,[⊥] and Rose Amal*[,†]

[†]School of Chemical Engineering, UNSW Australia, Sydney, New South Wales 2052, Australia

[‡]Department of Engineering, Macquarie University, Sydney, New South Wales 2109, Australia

[§]Mark Wainwright Analytical Centre, UNSW Australia, Sydney, New South Wales 2052, Australia

[∥]School of Chemistry, UNSW Australia, Sydney, New South Wales 2052, Australia

[⊥]School of Chemical and Biomolecular Engineering, The University of Sydney, Sydney, New South Wales 2006, Australia

Supporting Information

ABSTRACT: Fine metal nanoparticles (2−3 nm; Au, Pt, and alloyed Au−Pt) with a narrow size distribution were deposited on active TiO_2 through a facile chemical reduction method. Compared to the bare TiO_2, a remarkable enhancement of up to 10-fold for photocatalytic hydrogen evolution was achieved on the alloyed nanocomposites. By using core level and valence band XPS analysis, two electronic properties are shown to contribute to the promoted photocatalytic activity: stronger metal−support interaction between the alloyed structures and TiO_2 and higher electron population on the Au−Pt/TiO_2 photocatalysts in comparison with the bare TiO_2. Moreover, an improved charge separation over TiO_2 using Au−Pt nanoparticles was clearly evidenced by the significant increase of photocurrent responses obtained from the photoelectrochemical measurements. For the first time, in situ ^{13}C and ^{1}H NMR spectroscopy was applied to monitor the gas−liquid−solid photocatalytic reactions under real working conditions. Via a two-electron oxidation pathway, the surface-adsorbed methanol was first oxidized to formaldehyde, followed by spontaneous hydrolysis and methanolysis to methanediol and methoxymethanol, rather than methyl formate and formic acid that have been previously reported in gaseous CH_3OH photocatalysis. The in situ monitoring also revealed that deposition of metal NPs would not alter the reaction pathways while making the reaction faster compared to the bare TiO_2.

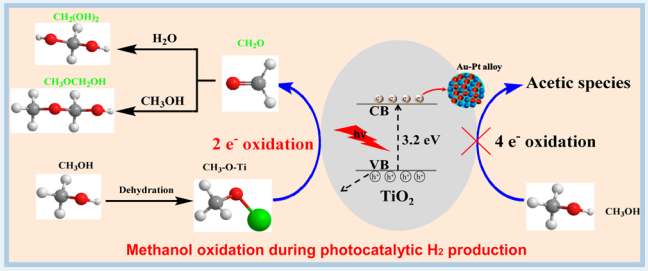

KEYWORDS: *hydrogen production, Au−Pt/TiO_2, valence band XPS, in situ photolysis NMR, molecular mechanism*

INTRODUCTION

Photocatalytic water splitting has long been targeted as an attractive way to store solar energy, as hydrogen (H_2) is a clean and portable fuel source.[1] Titanium dioxide (TiO_2) is one of the most studied photocatalysts owing to its low cost, nontoxicity, and abundance.[2] Notwithstanding, none of the existing bare TiO_2 materials available to date could produce H_2 from pure water due to the fast recombination of the photoinduced electron−hole pairs. To overcome this critical obstacle, the following two strategies are essentially used to facilitate efficient separation of the electron−hole pairs: (i) surface modification of TiO_2 with metals allows for efficient transfer of the photoexcited electrons to the surface sites;[3] (ii) addition of sacrificial reagents, commonly methanol, to scavenge the photogenerated holes.[4]

Deposition of metal nanoparticles (NPs) on the TiO_2 surface has been proven to be an efficient way to enhance the photoinduced charge separation due to their relatively higher work function compared to bare TiO_2.[5] To obtain stable and durable photocatalysts, the metals used in this approach should be photochemically inert. Among them, platinum (Pt), with the highest work function, has been widely used as a cocatalyst for H_2 generation because of its effective electron withdrawing from the TiO_2 conduction band and low overpotential toward the reduction of protons to produce H_2.[6] Gold (Au) NPs supported on TiO_2 have exhibited good activities in selective (photo)oxidation of hydrocarbons.[7] Moreover, Au, as a plasmonic metal that concentrates the light flux including UV and visible photons, forming hot spots surrounding the reaction surface sites, would effectively drive the endothermic reactions.[8] A previous study found that Au−Pt supported on commercial TiO_2 upon pre-reduction under H_2 at 500 °C can dramatically enhance H_2 production compared to the monometallic Au/TiO_2 and Pt/TiO_2 NPs.[9] It was suggested that the improved activity is the result of a combination of positive aspects. Due to the complexity of this multistep photochemical process in

Received: March 23, 2015
Revised: May 12, 2015
Published: May 13, 2015

DOI: 10.1021/acscatal.5b00623
ACS Catal. 2015, 5, 3924−3931

aqueous phase, however, experimental evidence for the role of these aspects is still lacking or ambiguous.

The use of sacrificial reagents, mainly methanol, is an effective way to scavenge the photoexcited holes and thus improve H_2 production. Studies on the methanol photochemistry in the gas−solid phase have been previously carried out. Frei's group found that the photoreaction of gaseous methanol with oxygen on the $FeAlPO_4$ material initially produced formaldehyde (HCHO) and hydrogen peroxide, and spontaneously transformed to formic acid, methyl formate ($HCOOCH_3$), and water as final products.[10] In the absence of O_2, Gu et al. observed the same species in methanol reforming over Sn−Ru/TiO_2 photocatalysts. Xu et al. revealed that the hydrogen released from UV photocatalysis of gaseous methanol on anatase TiO_2 occurred via photocatalytic dissociation of methanol followed by thermal recombination of dissociated protons on the bridge-bonded oxygen at above 400 K.[12]

As the photocatalytic hydrogen production from water takes place in an aqueous system with suspended solids, it has not been possible, to date, to monitor the three-phase reactions under light illumination by in situ spectroscopy, although the in situ solid-state ^{13}C NMR and FT-IR have been developed to study the adsorption and photoreactivity of gaseous methanol on solid catalysts in controlled reaction conditions. Monitoring photocatalytic reactions in liquid phase under real working conditions has been limited. In situ electron spin resonance (EPR) was recently used by Long et al. to monitor the change of the Ti^{3+} species and electron trapped oxygen vacancies under light irradiation at 77 K. In this study, we first applied in situ liquid NMR to simultaneously monitor the changes of methanol and water and their derived intermediates and products in the photocatalytic process under light irradiation at room temperature.

To the best of our knowledge, investigation of the molecular mechanism of this three-phase reaction under in situ photolysis has not yet been attempted. As methanol plays a crucial role in H_2 production, it is very demanding to get better understanding of the methanol-involved photocatalytic process under real working conditions. Recently, our isotopic tracer studies by gas chromatography isotope ratio mass spectroscopy (GC-IRMS) revealed the produced H_2 in aqueous phase mainly originated from water rather than methanol, while methanol was oxidized to formaldehyde and CO_2 in the oxygen-free conditions.[13] A better understanding of the photocatalytic process during hydrogen production, including adsorption/desorption of methanol and intermediate products is greatly needed to elucidate the reaction mechanism, knowledge of which can assist in improving overall efficiency.

In this work, the Au−Pt alloyed NPs deposited on our highly active TiO_2 by a facile chemical reduction method exhibited a 10-fold higher yield of hydrogen from water/CH_3OH mixture compared to the bare TiO_2. Both core level and valence band XPS spectra have evidenced that a stronger metal−support interaction and more electron-rich alloyed nanocomposites may contribute to the remarkably improved photocatalytic activity. Moreover, the photoelectrochemical measurements show that the bimetallic photocatalysts exhibit higher photocurrent response than their monometallic counterparts, which is an indication of more efficient photoinduced charge separation. We first introduce an in situ ^{13}C and ^{1}H liquid NMR technique that was employed to monitor the elementary reaction steps involved in a three-phase process of photocatalytic hydrogen production under real working conditions. We found that the formaldehyde formed from two-electron oxidation reaction underwent spontaneous hydrolysis and methanolysis to methanediol ($HOCH_2OH$) and methoxymethanol (CH_3OCH_2OH), rather than to methyl formate and formic acid observed in gas-phase CH_3OH photocatalysis.

EXPERIMENTAL SECTION

Catalyst Preparation. The bare TiO_2 NPs were synthesized through an evaporation-induced self-assembly method as we reported previously.[14] Briefly, 10 mL of titanium isopropoxide (TTIP) was added to 250 mL of Milli-Q water under vigorous stirring, and then the suspension was subjected to sonication for 30 min followed by aging for 2 days. Subsequently, the water was evaporated in air at 100 °C to afford a white powder, which was calcined at 500 °C for 1 h, giving well-crystallized TiO_2 particles. A chemical reduction method was utilized to prepare the Au, Pt, and Au−Pt-decorated TiO_2 composites keeping 1.0 wt % of total metal content. In a typical procedure, a nominal amount of metal precursor ($HAuCl_4{\cdot}3H_2O$ or/and $H_2PtCl_6{\cdot}H_2O$) was dissolved in Milli-Q water under stirring, followed by the addition of the synthesized TiO_2 particles. The suspension was then further stirred for 1.5 h in an ice bath. To ensure that smaller and more monodispersed NPs could be generated, an excess of ice cold $NaBH_4$ solution (0.1 M) was quickly injected into the suspension and further stirred for 3 h. The products were centrifuged and washed with ethanol and water, and dried at 110 °C. For comparison, bimetallic Au−Pt NPs were also deposited onto the commercial P25 TiO_2 from Degussa using the same procedure.

Structural Characterization. Transmission electron microscopy (TEM) images were obtained on a Philips CM200 microscope. Scanning TEM (STEM) was performed in a JEOL 2200FS TEM equipped with a high-angle annular dark field (HAADF) detector and a Bruker energy-dispersive spectrometer (EDS). The EDS analysis was operated using a nominal electron beam size of 1 nm. UV−vis diffuse reflectance spectra were obtained on a Shimadzu UV 3600 spectrophotometer. X-ray photoelectron spectroscopy (XPS) was conducted on an ESCALAB250Xi spectrometer (Thermo Scientific, U.K.) using a monochromated Al Kα X-ray radiation source at 15.2 kV and 168 W. The binding energies were calibrated on the basis of the hydrocarbon C1s peak at 285.0 eV. The spectra deconvolution was carried out by XPS PEAK41 software packages.

Photocatalytic Hydrogen Evolution. The experiments for photocatalytic hydrogen generation were carried out on a top-irradiation reactor with a 300 W xenon arc lamp. In a typical procedure, 50 mg of the prepared catalyst was dispersed in 100 mL of water/methanol mixture (volume ratio = 9/1) under sonication. Argon was purged into the system for more than 30 min to completely vent out the air. The mixture was then irradiated under magnetic stirring, and a water jacket was placed on the top of the reactor to absorb the heat. The evolved gas was analyzed every 30 min using a gas chromatograph (GC, Shimadzu, 8A) equipped with a thermal conductivity detector (TCD). In order to study the surface plasmon resonance (SPR) effect of metal nanostructures under visible light irradiation on the photocatalytic process, a cut-off optical filter of $\lambda > 420$ nm was used.

Photoelectrochemical (PEC) Measurements. The photoelectrodes were prepared by the drop-casting method. In a typical process, 2 mg of the catalyst was dispersed in 2 mL of ethanol by sonication, and then the suspension was dropped

DOI: 10.1021/acscatal.5b00623
ACS Catal. 2015, 5, 3924−3931

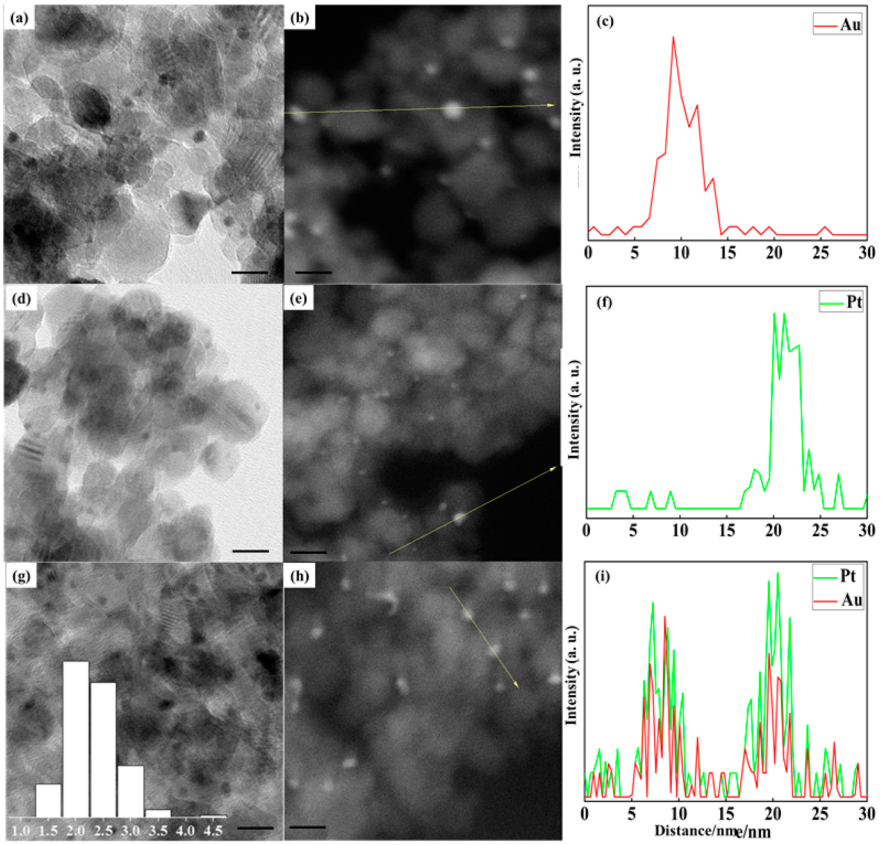

Figure 1. Representative TEM, HAADF-STEM images and the line-scan elemental profiles of the Au/TiO_2 (a, b, c), Pt/TiO_2(d, e, f), and Au−Pt/TiO_2 (g, h, (i), respectively. The inset of panel g is the size histogram of Au−Pt/TiO_2 NPs (scale bar: 10 nm).

onto fluorine-doped tin oxide glass (FTO, 2 cm × 1.5 cm) through a layer-by-layer method. Photocurrent measurements were undertaken in a 0.2 M Na_2SO_4 solution as electrolyte at room temperature by using an Autolab potentiostat (Model PGSTAT302N) with a bias of 0.3 V in a two-electrode PEC cell with Pt as the counter electrode and reference electrode and the catalyst-coated FTO glass as the working electrode. The electrolyte solution was purged with N_2 for 10 min prior to the measurement, and the purging was continued for the duration of photocurrent measurements to remove any dissolved O_2 in the cell. The photocurrent was then measured using a 300 W xenon lamp. To minimize the heat effect of the electrolyte solution under illumination, a water jacket was placed between the Xe lamp and the PEC cell.

In Situ Photolysis NMR Experiments. In situ photolysis NMR studies were performed on a Bruker Avance III 600 MHz NMR spectrometer using a 5 mm triple broadband inverse probe in locked mode at controlled temperatures. Typically, ca. 1 mg of the catalyst was dispersed in the mixture of 0.54 mL of D_2O, 0.03 mL of $^{13}CH_3OH$, and 0.03 mL of $^{12}CH_3OH$ with the assistance of sonication in darkness in a screw cap NMR tube fitted with a septum. Samples were irradiated by means of an Oriel Q-series lamp housing fitted with a 100 W Hg arc lamp and water filter focused onto a 2.5 m long, 1.5 mm diameter, UV-transmitting, single silica fiber optic. The fiber optic was inserted into the NMR tube through the septum, and then the tube was put into the NMR magnet.[15] ^1H and ^{13}C NMR spectra were acquired as a function of in situ photolysis time on the bare TiO_2 and bimetallic Au−Pt/TiO_2 catalyst, respectively. Spectra were recorded using a pulse width of 6 μs with a repetition time of 6 s. Water suppression was achieved using an excitation sculpting method.[16]

RESULTS

The size and morphology of the mono- and bimetallic TiO_2 NPs were analyzed by TEM and HAADF-STEM as shown in Figure 1. The images of monometallic Au/TiO_2 (Figure 1a, b) showed the spheroidal shaped gold NPs with a size of ca. 3 nm were well distributed on the surface of TiO_2. The composition line scanning profile through the bright spots (along a direction shown in Figure 1b) confirmed the presence of (Au) NPs along the TiO_2 (Figure 1c). In Figure 1d, the Pt metal supported on TiO_2 exhibited a slightly finer particle size of ca. 2 nm, which is consistent with the bright tiny spots in the HAADF-STEM image (Figure 1e). The corresponding line-scan elemental analysis exhibited the monometallic compositional characteristic, as shown in Figure 1f. From the TEM image of the bimetallic Au−Pt/TiO_2 NPs in Figure 1g, it was found that the metal NPs were also uniformly dispersed on the support, and the inset shows the histogram of the metal size distribution based on 200 NPs centered at 2−3 nm. The STEM image further confirmed the high dispersion and tiny size of the noble metal NPs. The line-scan elemental analysis profile through the metal NPs revealed the coexistence of Au and Pt with arbitrary composition, indicating the formation of homogeneous alloyed-structure in the bimetallic Au−Pt solid solution, which is consistent with our previous results.[17] Generally, Pt metal, with a low heat of surface energy compared to Au metal, has a tendency to accumulate on the surface, resulting in the presence of Pt as a shell on Au cores. However, the surface

DOI: 10.1021/acscatal.5b00623
ACS Catal. 2015, 5, 3924−3931

energy can also be related to the surrounding environment and the reducing agent used for the synthesis.

Figure 2 shows the UV−vis diffuse reflectance spectra of the samples in this study. The UV absorbance of TiO_2 at $\lambda < 400$ nm can be attributed to the intrinsic bandgap absorption. Compared to the bare TiO_2 materials, the spectrum of Pt/TiO_2 showed a broad absorption band at $\lambda > 400$ nm due to the interband transition of Pt NPs.[18] The Au/TiO_2 NPs exhibited an intense absorption band centered at 540 nm, which could be assigned to the SPR of the Au NPs.[7] We note that this SPR peak wavelength is slightly blue-shifted as compared to our previously reported Au/TiO_2 synthesized by a sol−gel hydrothermal method, suggesting a decrease of the Au particle size.[13] For the bimetallic system, the spectrum shows a fast flattening of the Au SPR band in the visible light region, which can be explained by the influence of strong metal−metal interactions at the alloy interface.[19] Obviously, the spectrum of $Au-Pt/TiO_2$ cannot be represented by a simple superposition of the spectra for the monometallic ones, further corroborating the formation of Au−Pt alloy composites.[20]

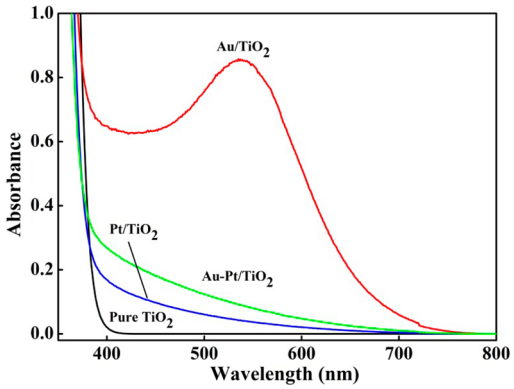

Figure 2. UV−vis diffuse reflectance spectra of the bare and metal-deposited TiO_2 photocatalysts.

Figure 3 depicts the amount of hydrogen evolved during the photocatalytic process over the bare and metallic TiO_2 compared to the benchmark Degussa P25 TiO_2 and its bimetallic photocatalyst. The activities of the metal-deposited photocatalysts are significantly higher than those for the metal-free ones. For instance, the bare TiO_2 produced only 364 μmole of H_2 after 3 h of irradiation. For the Au/TiO_2, 1493 μmole of H_2 was produced, while 2093 μmole of H_2 was detected when the Pt/TiO_2 catalyst was used. It must be stressed that the $Au-Pt/TiO_2$ catalyst delivered a H_2 production of 3550 μmole that is almost a 10-fold increase compared to the bare TiO_2. The bimetallic catalyst supported on P25 produced 2600 μmole of H_2 within 3 h illumination, whereas the bare P25 only produced 206 μmole of H_2 during the same period. Notably, all the photocatalysts used in this study produced only H_2 with the lack of O_2 evolution.

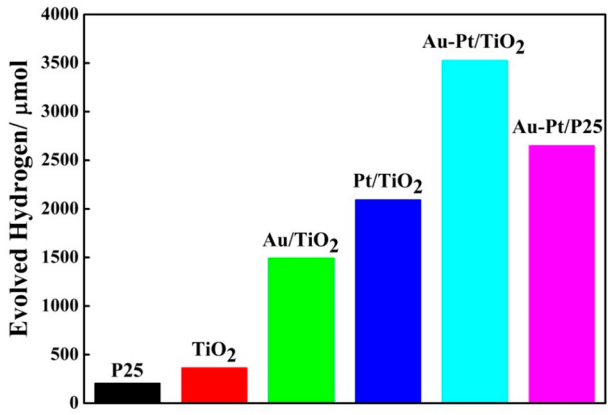

Figure 3. Hydrogen evolution on the bare and metallic TiO_2 photocatalysts using the benchmark Degussa P25 TiO_2 and its bimetallic materials as the references. Reaction condition: 50 mg catalyst in 100 mL of water/methanol solution (volume ratio = 9:1) and irradiation of 3 h.

The XPS results are shown in Figure 4. The gold in the Au/TiO_2 and $Au-Pt/TiO_2$ samples exists in metallic states, as indicated by the Au 4f spectra, which were composed of the Au $4f_{7/2}$ and Au $4f_{5/2}$ peaks (Figure 4a). Compared to the XPS data taken from bulk gold materials (84.0 eV), the Au $4f_{7/2}$ peaks were slightly shifted toward lower binding energy region with the Au/TiO_2 at 83.5 eV and the $Au-Pt/TiO_2$ at 83.4 eV, respectively, indicating a strong interaction between Au and the TiO_2 support.[21] Figure 4b shows the Pt 4f spectra of the Pt/TiO_2 and $Au-Pt/TiO_2$ samples. For the Pt/TiO_2 sample, the peaks centered at 71.1 and 74.5 eV can be assigned to the Pt $4f_{7/2}$ and Pt $4f_{5/2}$ levels of the Pt metallic state, respectively, and the peaks at 72.7 and 76.1 eV arise from Pt $4f_{7/2}$ and Pt $4f_{5/2}$ levels, indicating the coexistence of oxidized Pt species.[22] It seems that the Pt metallic state was predominant in the Pt/TiO_2. It is also noted that the Pt $4f_{7/2}$ peak is shifted to a lower energy region compared to the bulk Pt materials.[23] In the bimetallic materials, Pt in the zerovalent state was detected as the main species (70.7 eV for the Pt $4f_{7/2}$) along with a small amount of oxidized Pt species featured at 72.2 eV for the Pt $4f_{7/2}$ level, as seen in Figure 4b. The presence of the oxidized Pt species is probably caused by the oxidation of metallic Pt in the air prior to XPS analysis. Of particular note is that, in the bimetallic materials, the binding energies of Pt and Au were slightly lower by 0.4 and 0.1 eV compared to the corresponding monometallic Pt/TiO_2 and Au/TiO_2, respectively. This phenomenon showed that the metals in the alloyed system are more negatively charged, an indicator of stronger interaction between the metals and TiO_2 supports.

It has been accepted that the metal valence band structure can strongly depend on the electronic structure or coordination number of surface atoms. Figure 4c presents the XPS spectra in the valence band region of the bare and metallic TiO_2 photocatalysts. The edge of the maximum energy can be determined at ca. 2.8 eV, which is consistent with the reported values.[24] Deposition of the metal NPs does not cause any significant change in the valence band position of TiO_2. However, it is worth noting that the onset of the photoelectron's signal of the Pt/TiO_2 and $Au-Pt/TiO_2$ materials was lower than that for the bare TiO_2. This means that the counts of the electrons started from a lower energy region in the Pt and Au−Pt materials. Moreover, the population of the detected electrons from the $Au-Pt/TiO_2$ photocatalyst was higher than that of the monometal Pt/TiO_2 in the lower energy region, indicating that there are more electrons on alloyed nanostructures compared to the Pt/TiO_2, agreeing well with the core level XPS spectra of the metals.

The improved charge separation on the metal modified catalysts was further confirmed by the photocurrent responses in a two-electrode PEC cell. As shown in Figure 5, a fast and uniform photocurrent response was observed for all the

DOI: 10.1021/acscatal.5b00623
ACS Catal. 2015, 5, 3924−3931

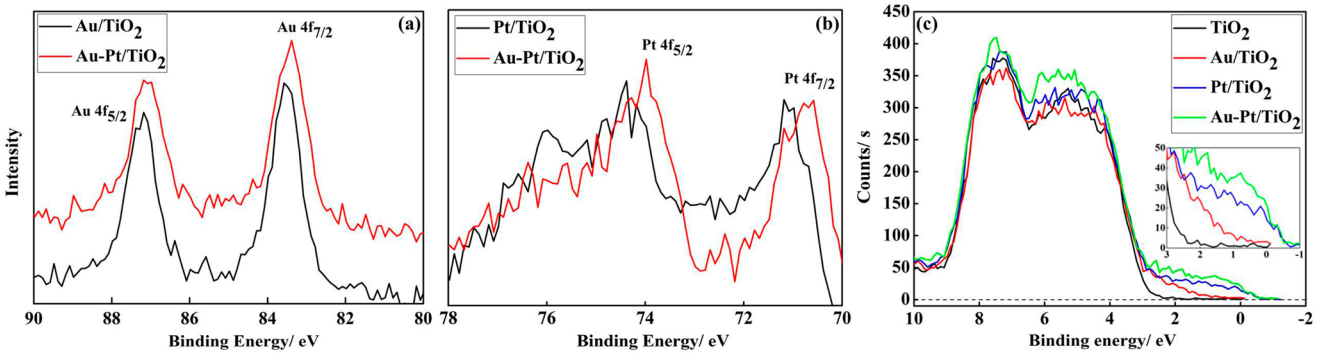

Figure 4. (a) XPS Au 4f spectra of the Au/TiO_2 and $Au–Pt/TiO_2$ samples, (b) XPS Pt 4f spectra of the Pt/TiO_2 and $Au–Pt/TiO_2$samples, and (c) valence band XPS spectra of the bare TiO_2 and metallic TiO_2 samples.

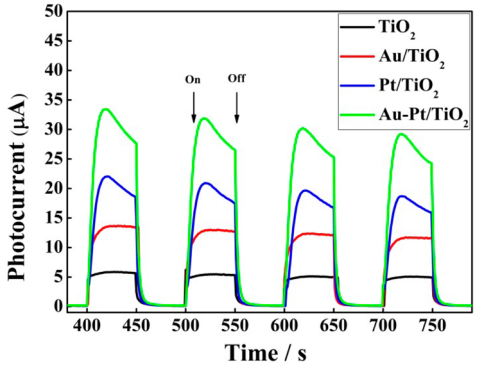

Figure 5. Photocurrent response (in chopping mode, light on–off repeatedly) of the bare and metal-deposited TiO_2 photocatalysts under UV–vis light irradiation (Xe Lamp 300W).

photocatalysts on each switch on/off cycle under irradiation. It can be clearly seen that the photocurrent response of the Au/TiO_2 coated electrode was enhanced compared to the bare TiO_2 electrode under light illumination. The photocurrent on the Pt/TiO_2 was even higher, indicating that the electron transportation from the conduction band of TiO_2 to Pt nanoparticles is more efficient, relative to that of Au nanoparticles. It is interesting to observe that the photocurrent obtained on $Au–Pt/TiO_2$ is greatly enhanced compared to its monometallic counterparts, which indicates that the separation of the photogenerated electron–hole pairs is greatly improved in the bimetallic systems. The photocurrent response of the bare and metal–TiO_2 catalysts under light irradiation obtained from Figure 5 is in the order of $Au–Pt/TiO_2$> Pt/TiO_2> Au/TiO_2> bare TiO_2, which coincides with that of the photocatalytic activity in hydrogen evolution. In the four-cycle measurement, similar photocurrent values were obtained in each switch on/off cycle, showing good reproducibility of the photocatalysts. The completely reproducible cycles of high photoresponsivity indicates that most of the photogenerated electrons could be transferred to the back contact across the material to produce photocurrent responses upon light irradiation.

For the bare and Au/TiO_2 samples, the photocurrent response rapidly increased and reached a constant value once the light was switched on. The gradual decrease of the photocurrent obtained on Pt/TiO_2 and $Au–Pt/TiO_2$ after switching on the light illumination indicates that the recombination of the photoinduced electron–hole pairs occurred in the process of irradiation. Upon light irradiation, plenty of electron–hole pairs would be generated. On the bare TiO_2, the photogenerated charge carriers would undergo fast recombination, thus leading to a low photocurrent, which results in less electron transfer from the working electrode to the counter electrode. A similar phenomenon was also observed on the Au/TiO_2, though the charge separation efficiency was largely improved. However, on the Pt/TiO_2 and $Au–Pt/TiO_2$, upon the generation of the photoexcited electron–hole pairs, the electrons can be efficiently trapped by the Pt and Au–Pt nanoparticles followed by transfer to the counter electrode. Unlike in the photocatalytic H_2 production process, where the holes can be consumed quickly by oxidizing the hole scavenger methanol, the photogenerated holes were accumulated on the working electrodes in the PEC measurement due to less efficient removal of holes during the process of water oxidation. Therefore, with the increase inillumination time, more recombination of the photoexcited electron–hole pairs is inevitable.[25] Consequently, photocurrent decay during each switch-on/off cycle was observed.

A detailed understanding of the photocatalytic cycle for H_2 production may provide the basis to improve the existing photocatalytic system and design new ones. In this study, we introduced high-resolution in situ photolysis ^{13}C and ^{1}H liquid NMR to simultaneously monitor the state of reactants, intermediates, and products in the photocatalytic process under the real working condition for the first time. Figure 6 shows a stacked plot of ^{13}C and ^{1}H NMR spectra recorded on a sample containing the $Au–Pt/TiO_2$ catalyst as a function of irradiation time. For comparison, the corresponding ^{13}C NMR spectra using the bare TiO_2 catalyst are presented in Figure S1. Prior to the light irradiation on the bare TiO_2, a dominant signal at 49 ppm was observed in the ^{13}C NMR spectrum (not shown), corresponding to $^{13}CH_3OH$ in the aqueous phase, and a tiny peak at 55 ppm (Figure S1, bottom), which is attributed to chemisorbed methoxy species ($^{13}CH_3–O–Ti$) onto the TiO_2 surface.[26] Prior to photolysis, the ^{1}H NMR spectra in Figure S2 (bottom) only gave the signals of H_2O and methanol. At the start of light irradiation on the bare TiO_2, three new signals at 83, 90, and 54.5 ppm, assigned to methanediol ($HO^{13}CH_2OH$) and methoxymethanol ($^{13}CH_3O^{13}CH_2OH$) are presented in Figure S1 (top). For the $Au–Pt/TiO_2$, the ^{13}C NMR spectrum in Figure 6a presents both signals of methanediol and methoxymethanol at 83 and 90 ppm.[27] The identification of the products was confirmed by two-dimensional heteronuclear single quantum coherence ($^{1}H–^{13}C$ HSQC) and heteronuclear multiple bond correlation

DOI: 10.1021/acscatal.5b00623
ACS Catal. 2015, 5, 3924–3931

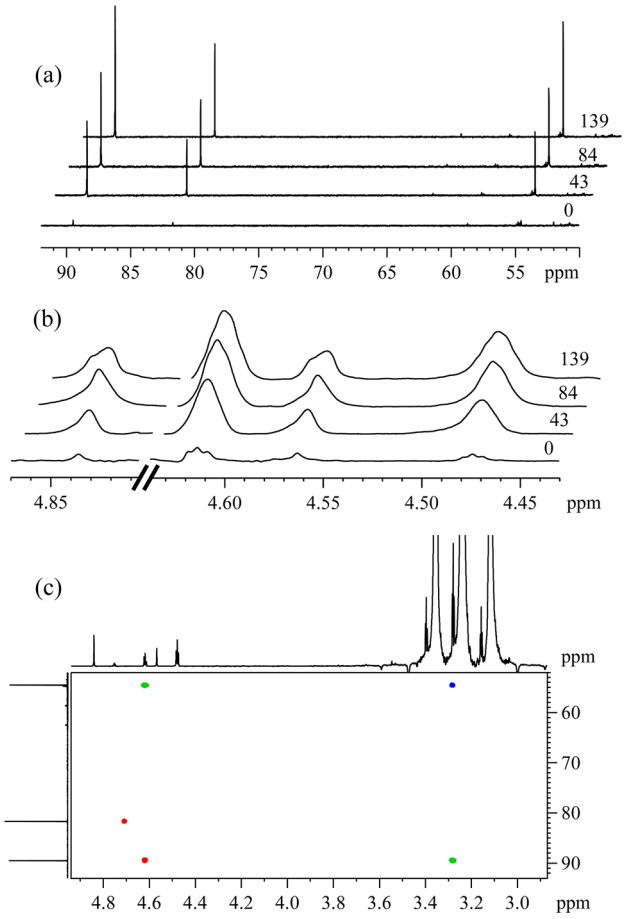

Figure 6. (a) ^{13}C NMR and (b) ^{1}H NMR spectra recorded during the photocatalytic hydrogen production on the Au−Pt/TiO_2 using a mixture of D_2O and $^{13}CH_3OH/^{12}CH_3OH$ and as a function of in situ irradiation time, and (c) overlay of $^{1}H-^{13}C$ HSQC (single bond, red CH_2, and blue CH_3) and HMBC (multiple bond, green) correlation spectra of the suspension sample after light irradiation of 139 min. Annotated with a solvent suppressed ^{1}H NMR spectrum in f_2.

($^{1}H-^{13}C$ HMBC) experiments, as shown in Figure 6c and multiplet analysis of the ^{13}C spectrum in Figure S3−S7.

As the photocatalytic reaction proceeded, the peak intensity of both methanediol and methoxymethanol increased. The stacked ^{1}H NMR spectra presented in Figure 6b also indicated the appearance and accumulation of methanediol and methoxymethanol during the photocatalytic process. As the reaction progresses, ^{13}C NMR monitoring gave increased intensities of the intermediate peaks and the occurrence of the final product, $^{13}CO_2$ as shown in Figure S3. On both materials, no evidence of formate or acids was observed from methanol photocatalysis in the aqueous phase. It indicates that the metal deposition did not alter the methanol oxidation process.

DISCUSSION

Compared to the benchmark P25 TiO_2, our bare TiO_2 exhibited a higher activity in H_2 generation both with and without the presence of metals, suggesting the superior activity of the bare TiO_2 materials. Our previous solid-state ^{1}H NMR results revealed that the number of terminal hydroxyl groups on the TiO_2 surface is vital for determining its photocatalytic activity: low terminal hydroxyl group content accounts for the high activity.[28] The bare TiO_2 used in this work was accordingly synthesized with a modified procedure to eliminate the terminal hydroxyl groups on the TiO_2 surface.[14] It exhibited a 100 % photodegradation rate of various organic compounds on account of its unique acidic properties on the surface, which could promote the adsorption and subsequent oxidation of organics, showing better activity than the P25. In this study, it could be understood that the methanol molecules strongly adsorbed on these acidic sites and efficiently captured the photogenerated holes in the valence band of TiO_2 and could be instantaneously oxidized.

On the other hand, noble metals including Au, Pd, and Pt NPs supported on the semiconductor surface have been extensively used to trap photoinduced electrons.[22] In the absence of metal, the photoinduced electrons migrate to the surface and are trapped by the surface Ti^{4+}, forming Ti^{3+}, and thus, the number of electrons available for the reduction of hydrogen ions decreases, leading to lower hydrogen production.[4] The presence of metal, in particular the noble metals with a larger work function, namely, lower Fermi level, can efficiently trap the photoinduced electrons to be involved in the reduction of hydrogen ions, improving the charge carrier separation.[5b] Among these noble metals, Pt has the largest work function, and thus, better photocatalytic activity is always expected, as seen in the present study. For the Au/TiO_2 photocatalyst, Au NPs that support the SPR when interacting with UV and visible photons can promote the formation of electron−hole pairs in the semiconductor by the SPR excitation.

To investigate the SPR effect of the AuNPs on the H_2 generation, visible irradiation of $\lambda > 420$ nm was applied while the other reaction conditions were kept constant. After 5 h of irradiation, no hydrogen but only a trace of CO_2 (0.3 μmole) was detected. This finding is consistent with the previous study that used the irradiation at 550 ± 20 nm to excite the Au SPR.[29] Naldoni et al. reported the notable generation of hydrogen under visible light irradiation was achieved on the Au/black TiO_2 heterostructures.[30] The efficient electron transfer from the Au nanoparticles can be attributed to the synergistic effect between the intraband gap electronic levels of the black TiO_2 and the Au interband and SPR transitions under visible light irradiation. In the present study, however, no hydrogen but only a trace of CO_2 was produced, suggesting that the SPR effect of Au NPs triggered the oxidation of methanol but not the reduction of protons under visible light irradiation; the Au NPs on the TiO_2 surface might mainly act as the electron traps under UV light. As can be seen from the enhanced hydrogen generation on the bimetallic catalysts, the addition of Pt in the alloyed structure played an important role in the reduction of protons to produce H_2, which might be due to the suitable Fermi level of the alloyed metal nanoparticles relative to the conduction band of TiO_2 and the weakened hydrogen−metal bond, which favors the easy diffusion of the produced hydrogen from the surface of the bimetallic nanoparticles.[31]

From the XPS studies on the surface and electronic structure, the enhancement in the photocatalytic H_2 generation on the bimetallic TiO_2 could be attributed to the stronger interaction between alloyed NPs and the support. Our results demonstrated that both the binding energies of Pt and Au in the alloyed NPs were shifted toward the lower energy regions compared to the monometallic Pt/TiO_2 and Au/TiO_2. This indicates that the metals in the alloyed system were more negatively charged, which might be caused by a decrease of the coordination number of surface Pt atoms and strong interaction

DOI: 10.1021/acscatal.5b00623
ACS Catal. 2015, 5, 3924−3931

Scheme 1. Methanol and Its Dissociative Species Underwent Two-Electron Oxidation to Produce Formaldehyde and Its Spontaneous Hydrolysis and Methanolysis Product in Photocatalytic H_2 Production Process Inferred from the in Situ Photolysis NMR Results

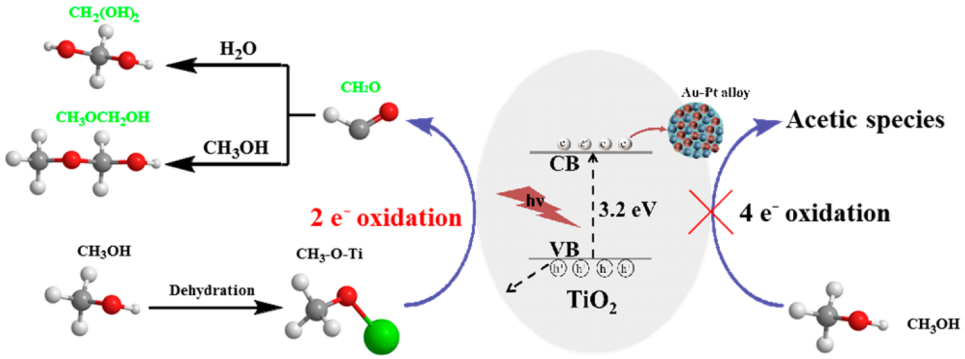

of Pt and Au NPs with the TiO_2 support.[32] This strong metal−support interaction could induce weakening the bond between H_2 molecules and the Au−Pt alloy-structured interfaces. It could facilitate the desorption of produced H_2 molecules readily from the surface sites, thus leading to the enhanced activity.[33] The thermal desorption studied by mass spectrometer revealed that the H_2 molecules were more loosely bound on the Au−Pt alloy thin films than on the pure Pt ones.[34] The XPS results from van Bokhoven's group have also provided evidence on the weaker interaction of H_2 with the Au−Pt alloy clusters compared to the single Pt clusters on the supports Al_2O_3 and SiO_2.[35] It has been proposed that this weak bond was attributed to the ensemble-size effect arising from band rehybridization between the two metals. This finding can resemble our activity results that the H_2 molecules were more easily evolved from the bimetallic alloyed structures compared to the single metal Pt/TiO_2, due to the weaker H-metal bound state in the alloys. Therefore, the easy desorption of produced H_2 from the bimetallic catalysts probably played a significant role in boosting the hydrogen production. Moreover, our valence band XPS studies also provided the experimental evidence that the alloyed structure possesses higher *d*-band center energies (rich electrons) compared to the single metal TiO_2, which could be considered to be responsible for the remarkably enhanced photocatalytic activity.

Furthermore, a significant increase in photocurrent response by 5−6-fold was observed for the Au−Pt alloyed TiO_2 photocatalysts compared to that of the bare TiO_2 in the PEC measurements, indicating enhanced charge separation by using Au−Pt alloyed nanoparticles that contributes to the accelerated evolution of hydrogen in the photocatalysis system. Pt has the largest work function among all the noble metals, and Au has a smaller work function. After the band hybridization between Au and Pt, a suitable height of the Schottky energy barrier between TiO_2 and the bimetallic nanoparticles can be formed, which favors fast interfacial electron injection from the conduction band of TiO_2 to the metal nanoparticles. Hence, the metal nanoparticles deposited on the surface of TiO_2 can also work as electron mediator as well as cocatalysts in photocatalytic H_2 production.

As above-mentioned, the amount of photocatalytic H_2 production is about 10-fold higher on the alloyed photocatalyst than the bare TiO_2. It is worth noting that our recent isotopic tracer studies by GC-IRMS have revealed that the evolved H_2 molecules mainly originated from water rather than methanol. The latter was oxidized to formaldehyde and further to CO_2 detected by HPLC.[13] In the present work, a key achievement of the in situ photolysis ^{13}C NMR experiments is the direct observation of methanediol and methoxymethanol and no evidence for the formation of acetates or acids. The previous FT-IR spectra have shown the formation of four-electron-transfer product, acetate (−COO−) by the hole oxidation of methanol in the gas phase. It suggests the reaction pathway differs significantly from that observed here in aqueous phase that is the real working condition.

Based on the in situ photolysis NMR results, the photocatalytic H_2 production in a water/methanol system is proposed in Scheme 1. First, the methanol molecule adsorbed on titanium hydroxyl sites (Ti−OH) to form surface methoxy species (CH_3−O-Ti). In the absence of O_2, the methoxy species are indirectly oxidized by the photogenerated holes or hydroxyl radicals (·OH) which are products of the trapping photogenerated holes by the surface Ti−OH groups or adsorbed water molecules.[36] The resulting two-electron oxidation product, formaldehyde was highly reactive and therefore instantaneously reacted with water forming methanediol or with methanol giving methoxymethanol, respectively. The fast consumption of the produced formaldehyde drives the oxidation of methanol, and thus the photoinduced holes can be removed quickly from the surface of TiO_2. On the other hand, the photoexcited electrons in the conduction band can be efficiently transferred to the noble metal NPs. The corresponding protons obtained from photodissociation of adsorbed water molecules were easily reduced by these electrons. The Au−Pt alloyed-TiO_2 nanocomposites allow for a facile electron migration from the conduction band of TiO_2 to the metal nanoparticles and lower the activation energy of the half reactions, thus markedly boosting the hydrogen evolution. Therefore, a 10-fold enhanced hydrogen production was achieved on this multifunctional nanocomposite when compared to the bare TiO_2, but following the same reaction pathway.

CONCLUSION

In this work, bimetallic Au−Pt NPs deposited on the active TiO_2 prepared through a facile chemical reduction method exhibited a 10-fold photocatalytic H_2 evolution compared to the bare TiO_2 materials. Our experimental evidence demonstrate that the improved activity could come from a combination of positive morphological and electronic features including fine metal NPs (2−3 nm) with narrow size distribution, homogeneously alloyed nanostructure, strong

DOI: 10.1021/acscatal.5b00623
ACS Catal. 2015, 5, 3924−3931

metal−support interaction between the alloys and active TiO_2, and their electron richness. In situ monitoring of photocatalytic H_2 production under real working condition by ^{13}C and ^{1}H NMR spectroscopy was first employed to study the elementary multistep in the three-phase process. Methanol and its dissociative species underwent two-electron oxidation to produce formaldehyde and its spontaneous hydrolysis and methanolysis product, rather than four-electron oxidation products. The results show that metal deposition did not alter the reaction pathways but accelerated the reaction rate. This study presents a facile method for the preparation of highly active photocatalysts and advances our understanding of the elementary reaction steps for photocatalytic H_2 production under real working conditions.

■ ASSOCIATED CONTENT

Supporting Information

The Supporting Information is available free of charge on the ACS Publications website at DOI: 10.1021/acscatal.5b00623.

In situ photolysis ^{13}C and ^{1}H NMR spectra using the bare TiO_2 as photocatalyst, multiplet analysis of the ^{13}C spectra recorded on in situ photolysis of Au-Pt/TiO_2 suspension, and Ti_2p core-level XPS, ^{1}H MAS NMR, and FTIR spectra (PDF)

■ AUTHOR INFORMATION

Corresponding Authors

*E-mail: yijiao.jiang@mq.edu.au. Tel.: +612-9850-9535 Fax: +612-9850-9128.

*E-mail: r.amal@unsw.edu.au.

Notes

The authors declare no competing financial interest.

■ ACKNOWLEDGMENTS

Financial support through the ARC Discovery Early Career Researcher Award (DE120100329) and ARC Discovery Project (DP140102432) are gratefully acknowledged. We also thank the UNSW Mark Wainwright Analytical Centre at UNSW Australia for use of facilities.

■ REFERENCES

(1) Fujishima, A.; Honda, K. *Nature* **1972**, *238*, 37−38.

(2) Kudo, A.; Miseki, Y. *Chem. Soc. Rev.* **2009**, *38*, 253−278.

(3) Teoh, W. Y.; Scott, J. A.; Amal, R. *J. Phys. Chem. Lett.* **2012**, *3*, 629−639.

(4) Schneider, J.; Bahnemann, D. W. *J. Phys. Chem. Lett.* **2013**, *4*, 3479−3483.

(5) (a) Choi, W.; Termin, A.; Hoffmann, M. R. *J. Phys. Chem.* **1994**, *98*, 13669−13679. (b) Yang, J.; Wang, D.; Han, H.; Li, C. *Acc. Chem. Res.* **2013**, *46*, 1900−1909. (c) Bahruji, H.; Bowker, M.; Davies, P. R.; Kennedy, J.; Morgan, D. J. *Int. J. Hydrogen Energy* **2015**, *40*, 1465−1471.

(6) (a) Wu, M. C.; Hiltunen, J.; Sapi, A.; Avila, A.; Larsson, W.; Liao, H. C.; Huuhtanen, M.; Toth, G.; Shchukarev, A.; Laufer, N.; Kukovecz, A.; Konya, Z.; Mikkola, J. P.; Keiski, R.; Su, W. F.; Chen, Y. F.; Jantunen, H.; Ajayan, P. M.; Vajtai, R.; Kordas, K. *ACS Nano* **2011**, *5*, 5025−5030. (b) Bamwenda, G. R.; Tsubota, S.; Nakamura, T.; Haruta, M. *J. Photochem. Photobiol., A* **1995**, *89*, 177−189.

(7) Primo, A.; Corma, A.; Garcia, H. *Phys. Chem. Chem. Phys.* **2011**, *13*, 886−910.

(8) (a) Christopher, P.; Xin, H.; Marimuthu, A.; Linic, S. *Nat. Mater.* **2012**, *11*, 1044−1050. (b) Long, J.; Chang, H.; Gu, Q.; Xu, J.; Fan, L.; Wang, S.; Zhou, Y.; Wei, W.; Huang, L.; Wang, X.; Liu, P.; Huang, W. *Energy Environ. Sci.* **2014**, *7*, 973−977.

(9) Gallo, A.; Marelli, M.; Psaro, R.; Gombac, V.; Montini, T.; Fornasiero, P.; Pievo, R.; Dal Santo, V. *Green Chem.* **2012**, *14*, 330−333.

(10) (a) Yeom, Y.-H.; Frei, H. *J. Phys. Chem. A* **2002**, *106*, 3350−3355. (b) Ulagappan, N.; Frei, H. *J. Phys. Chem. A* **2000**, *104*, 490−496.

(11) Gu, Q.; Long, J.; Fan, L.; Chen, L.; Zhao, L.; Lin, H.; Wang, X. *J. Catal.* **2013**, *303*, 141−155.

(12) (a) Xu, C.; Yang, W.; Guo, Q.; Dai, D.; Chen, M.; Yang, X. *J. Am. Chem. Soc.* **2014**, *136*, 602−605. (b) Xu, C.; Yang, W.; Guo, Q.; Dai, D.; Chen, M.; Yang, X. *J. Am. Chem. Soc.* **2013**, *135*, 10206−10209.

(13) Yu, J.; Wang, K.; Xiao, W.; Cheng, B. *Phys. Chem. Chem. Phys.* **2014**, *16*, 11492−11501.

(14) Jiang, Y.; Amal, R. *Appl. Catal., B* **2013**, *138−139*, 260−267.

(15) Geftakis, S.; Ball, G. E. *J. Am. Chem. Soc.* **1998**, *120*, 9953−9954.

(16) Hwang, T. L.; Shaka, A. J. *J. Magn. Reson., Ser. A* **1995**, *112*, 275−279.

(17) Wang, F.; Jiang, Y.; Wen, X.; Xia, J.; Sha, G.; Amal, R. *ChemCatChem* **2013**, *5*, 3557−3561.

(18) Shiraishi, Y.; Tsukamoto, D.; Sugano, Y.; Shiro, A.; Ichikawa, S.; Tanaka, S.; Hirai, T. *ACS Catal.* **2012**, *2*, 1984−1992.

(19) Liz-Marzan, L. M.; Philipse, A. P. *J. Phys. Chem.* **1995**, *99*, 15120−15128.

(20) De, G.; Rao, C. N. R. *J. Mater. Chem.* **2005**, *15*, 891−894.

(21) (a) Wang, X.; Waterhouse, G. I. N.; Mitchell, D. R. G.; Prince, K.; Caruso, R. A. *ChemCatChem* **2011**, *3*, 1763−1771. (b) Arabatzis, I. M.; Stergiopoulos, T.; Andreeva, D.; Kitova, S.; Neophytides, S. G.; Falaras, P. *J. Catal.* **2003**, *220*, 127−135.

(22) Young, C.; Lim, T. M.; Chiang, K.; Scott, J.; Amal, R. *Appl. Catal., B* **2008**, *78*, 1−10.

(23) Alnot, M.; Gorodetskii, V.; Cassuto, A.; Ehrhardt, J. J. *Thin Solid Films* **1987**, *151*, 251−262.

(24) (a) Chen, X.; Liu, L.; Yu, P. Y.; Mao, S. S. *Science* **2011**, *331*, 746−750. (b) Liu, G.; Sun, C.; Yang, H. G.; Smith, S. C.; Wang, L.; Lu, G. Q.; Cheng, H.-M. *Chem. Commun.* **2010**, *46*, 755−757.

(25) (a) Xiang, Q.; Yu, J.; Jaroniec, M. *Nanoscale* **2011**, *3*, 3670−3678. (b) Yu, J.; Dai, G.; Huang, B. *J. Phys. Chem. C* **2009**, *113*, 16394−16401.

(26) Jiang, Y.; Huang, J.; Dai, W.; Hunger, M. *Solid State Nucl. Magn. Reson.* **2011**, *39*, 116−141.

(27) Hahnenstein, I.; Hasse, H.; Kreiter, C. G.; Maurer, G. *Ind. Eng. Chem. Res.* **1994**, *33*, 1022−1029.

(28) Jiang, Y.; Scott, J.; Amal, R. *Appl. Catal., B* **2012**, *126*, 290−297.

(29) Zhang, Z.; Wang, Z.; Cao, S.-W.; Xue, C. *J. Phys. Chem. C* **2013**, *117*, 25939−25947.

(30) Naldoni, A.; Fabbri, F.; Altomare, M.; Marelli, M.; Psaro, R.; Selli, E.; Salviati, G.; Dal Santo, V. *Phys. Chem. Chem. Phys.* **2015**, *17*, 4864−9.

(31) Gallo, A.; Montini, T.; Marelli, M.; Minguzzi, A.; Gombac, V.; Psaro, R.; Fornasiero, P.; Dal Santo, V. *ChemSusChem* **2012**, *5*, 1800−11.

(32) Wang, X.; Yu, J. C.; Yip, H. Y.; Wu, L.; Wong, P. K.; Lai, S. Y. *Chem. - Eur. J.* **2005**, *11*, 2997−3004.

(33) Hoffmann, M. R.; Martin, S. T.; Choi, W.; Bahnemann, D. W. *Chem. Rev.* **1995**, *95*, 69−96.

(34) Stephan, J. J.; Ponec, V.; Sachtler, W. M. H. *Surf. Sci.* **1975**, *47*, 403−412.

(35) Bus, E.; van Bokhoven, J. A. *Phys. Chem. Chem. Phys.* **2007**, *9*, 2894−2902.

(36) Wang, C.-Y.; Groenzin, H.; Shultz, M. J. *J. Am. Chem. Soc.* **2004**, *126*, 8094−8095.

DOI: 10.1021/acscatal.5b00623
ACS Catal. 2015, 5, 3924−3931